

# Unimorph deformable mirror for space telescopes: environmental testing

Peter Rausch,\* Sven Verpoort, and Ulrich Wittrock

Photonics Laboratory, Münster University of Applied Sciences  
Stegerwaldstraße 39, 48565 Steinfurt, Germany

[\\*rausch@fh-muenster.de](mailto:*rausch@fh-muenster.de)

**Abstract:** We have developed and manufactured a unimorph deformable mirror for space telescopes based on piezoelectric actuation. The mirror features 44 actuators, has an aperture of 50 mm, and is designed to reproduce low-order Zernike modes with a stroke of several tens of  $\mu\text{m}$ . We assessed the space compliance by operating the mirror in thermal vacuum, and exposing it to random and sinusoidal vibrations, as well as to ionizing irradiation. Additionally, the operational life time and the laser power handling capability were tested. The mirror was successfully operated in thermal vacuum at 100 K. We report on the conducted tests and the methods used to evaluate the mirror's performance, and discuss the compliance with the demanded requirements.

© 2016 Optical Society of America

**OCIS codes:** (010.1080) Active or adaptive optics; (110.6770) Telescopes; (120.6085) Space instrumentation; (120.6810) Thermal effects; (120.7280) Vibration analysis; (350.5610) Radiation; (350.6090) Space optics.

---

## References and links

1. H. W. Babcock, "The possibility of compensating astronomical seeing," *Publ. Astron. Soc. Pac.* **65**(386), 229–236 (1953).
2. F. Roddier, *Adaptive Optics in Astronomy* (Cambridge University, 1999).
3. J. Liang, D. R. Williams, R. David, and D. T. Miller, "Supernormal vision and high-resolution retinal imaging through adaptive optics," *J. Opt. Soc. Am. A* **14**(11), 2884–2892 (1997).
4. M. Booth, "Adaptive optics in microscopy," *Philos. T. Roy. Soc. A* **356**(1861), 2829–2843 (2007).
5. F. M. Dickey, T. E. Lizotte, S. C. Holswade, and D. L. Shealy, *Laser Beam Shaping Applications* (CRC, 2005).
6. R. Tyson, *Principles of Adaptive Optics* (CRC, 2010).
7. J. P. Gardner, J. C. Mather, M. Clampin, R. Doyon, M. A. Greenhouse, H. B. Hammel, J. B. Hutchings, P. Jakobsen, S. J. Lilly, K. S. Long, J. I. Lunine, M. J. McCaughrean, M. Mountain, J. Nella, G. H. Rieke, M. J. Rieke, H.-W. Rix, E. P. Smith, G. Sonneborn, M. Stiavelli, H. S. Stockmann, R. A. Windhorst, and G. S. Wright, "The James Webb Space Telescope," *Space Sci. Rev.* **123**(4), 485–606 (2006).
8. J. Fanson, and M. Ealey, "Articulating fold mirror for the Wide-Field/Planetary Camera II," *Proc. SPIE* **1920**, 306–316 (1993).
9. G. Hickey, T. Barbee, M. Ealey, and D. Redding, "Actuated hybrid mirrors for space telescopes," *Proc. SPIE* **7731**, 773120 (2010).
10. L. Gambicorti, F. D'Amato, F. Lisi, A. Riccardi, C. Vettore, F. Duo, A. Guercia, D. Gallieni, P. Lazzarini, M. Tintori, C. Patauner, R. Biasi, A. Zuccaro Marchi, and J. Pereira do Carmo, "Last results of technological developments for ultra-lightweight, large aperture, deployable mirror for space telescopes," in *Proceedings of the 9<sup>th</sup> International Conference on Space Optics (ICSO)*, Ajaccio, Corse (2012).
11. S. Manhart, W. J. Hupfer, S. Nikolov, C. Wuehrer, G. V. Vdovin, and Z. Sodnik, "50-mm MEMS deformable mirror," *Proc. SPIE* **4007**, 555–562 (2000).
12. H. Dyson, R. Sharples, N. Dipper, G. Vdovin, "Cryogenic wavefront correction using membrane deformable mirrors," *Opt. Express* **8**(1), 17–26, (2001).
13. M. A. Helmbrecht, T. Juneau, M. Hart, and N. Doble, "Segmented MEMS deformable-mirror technology for space applications," *Proc. SPIE* **6223**, 622305 (2006).

14. J. B. Stewart, T. G. Bifano, S. Cornelissen, P. Bierden, B. M. Levine, and T. Cook, "Design and development of a 331-segment tip-tilt-piston mirror array for space-based adaptive optics," *Sens. Actu. A-Phys.* **138**(1), 230–238 (2007).
15. K. Enya, H. Kataza, and P. Bierden, "A micro electrical mechanical systems (MEMS)-based cryogenic deformable mirror," *Publ. Astron. Soc. Pac.* **121**(877), 260–265, (2009).
16. C. B. Mendillo, B. A. Hicks, T. A. Cook, T. G. Bifano, D. A. Content, B. F. Lane, B. M. Levine, D. Rabin, S. R. Rao, R. Samuele, E. Schmidlin, M. Shao, J. K. Wallace, and S. Chakrabarti, "PICTURE: a sounding rocket experiment for direct imaging of an extrasolar planetary environment," *Proc. SPIE* **8442**, 84420E (2012).
17. M. L. Mulvihill, M. E. Roche, J. L. Cavaco, R. J. Shawgo, Z. Chaudhry, and M. A. Ealey, "Cryogenic deformable mirror technology development," *Proc. SPIE* **5172**, 60–67 (2003).
18. M. Laslandes, E. Hugot, M. Ferrari, C. Hourtoule, C. Singer, C. Devilliers, C. Lopez, and F. Chazallet, "Mirror actively deformed and regulated for applications in space: design and performance," *Opt. Eng.* **52**(9), 091803 (2013).
19. J.-C. Sinquin, A. Bastard, E. Beaufort, T. Berkefeld, L. Cadiergues, V. Costes, R. Cousty, C. Dekhtiar, F. Di Gesu, X. Gilbert, C. Grezes-Besset, D. Groeninck, M. Hartung, H. Krol, A. Moreau, P. Morin, H. Pages, R. Palomo, G. Scharmer, D. Soltau, and J.-P. Veran, "Recent results and future DMs for astronomy and for space applications at CILAS," *Proc. SPIE* **9148**, 91480G (2014).
20. K. Patterson and S. Pellegrino, "Ultralightweight deformable mirrors," *Appl. Opt.* **52**(22), 5327–5341 (2013).
21. P. Rausch, S. Verpoort, and U. Wittrock, "Unimorph deformable mirror for space telescopes: design and manufacturing," *Opt. Express* **23**(15), 19469–19477 (2015).
22. S. Verpoort, P. Rausch, and U. Wittrock, "Novel unimorph deformable mirror for space applications," in *Proceedings of the 9<sup>th</sup> International Conference on Space Optics (ICSO)*, Ajaccio, Corse (2012).
23. Secretariat, E.C.S.S. *Space Engineering Testing*, Technical Report ECSS-E-10-03A, ESA-ESTEC Requirements & Standards Division (2002).
24. J. Wyant, and K. Creath, "Basic wavefront aberration theory for optical metrology," in *Applied Optics and Optical Engineering*, Vol XI, Chap 1 (Academic, 1992).
25. X. L. Zhang, Z. X. Chen, L. E. Cross, and W. A. Schulze, "Dielectric and piezoelectric properties of modified lead titanate zirconate ceramics from 4.2 to 300 K," *J. Mater. Sci.* **18**(4), 968–972 (1983).
26. M. Nicolai, S. Uhlig, A. Schönecker, and A. Michaelis, "Experimental investigation of non-linear behaviour of PZT piezoceramics at low temperatures," *Adv. Sci. Tech.* **56**, 105–110 (2009).
27. M. Goy, C. Reinlein, J. Kinast, and N. Lange, "Cryogenic testing of a unimorph-type deformable mirror and theoretical material optimization," *J. Micro. Nanolithogr. MEMS MOEMS* **13**(1), 011107 (2014).
28. C. Reinlein, M. Goy, N. Lange, and J. Kinast, "Unimorph-type deformable mirror for cryogenic telescopes," *Proc. SPIE*, **9151**, 915104 (2014).
29. S. Verpoort, "Entwicklung neuartiger deformierbarer Spiegel für den Einsatz in Hochleistungslasern," Verlag Dr. Hut, (2011).
30. Arianespace, "Soyuz user's manual," Issue 2, <http://www.arianespace.com/wp-content/uploads/2015/09/Soyuz-Users-Manual-March-2012.pdf>.
31. J. J. Wijker, *Spacecraft Structures* (Springer Science & Business Media, 2008).
32. G. H. Broomfield, "The effects of temperature and irradiation on piezoelectric acoustic transducers and materials," AERE-R 11942 (1985).
33. T. Fett, S. Müller, D. Munz, and G. Thun, "Nonsymmetry in the deformation behaviour of PZT," *J. Mater. Sci. Lett.* **17**(4), 261–265 (1998).

---

## 1. Introduction

First proposed by Babcock in 1953 [1], systems for active wavefront control matured in the 1990 years. Mainly used in large ground-based telescopes to correct for atmospheric turbulences [2], the potential of adaptive optics to improve image quality in microscopy and ophthalmology, and to control laser beam profiles, soon became apparent [3–5]. The term "adaptive optics system" usually refers to systems having large correction bandwidths, sometimes up to several kHz. To distinguish these from systems which operate with correction bandwidths of 1 Hz or less, the term "active optics system" is often used [6]. The wavefront corrector(s) in an active or adaptive optics system are sometimes referred to as "the" active optics. Today, most major ground based telescopes are equipped with an adaptive optics system for atmospheric compensation. These systems are considered a key component of the telescope, rather than merely an add-on. Telescopes having a segmented primary mirror, such as the W. M. Keck Telescope, additionally employ active optics systems to align their mirror segments.

Active optics for space telescopes faces different challenges than adaptive optics for ground-based telescopes. In a space telescope, the main source of wavefront errors are distortions of the primary mirror. The design of space telescopes with large primary mirrors requires structures that are segmented and lightweight, since the primary mirror's mass and size are limited by the constraints imposed by the launch vehicle. Lightweight structures are prone to deformation due to thermally induced stress, mounting stress, and stress due to gravitational release. Beside the aberrations of a warped primary, deformations of the telescope structure may generate additional aberrations. Active optics ease the requirements on the rigidity of the optical train, and allow for on-site correction of aberrations.

On-site alignment is already considered a necessity, especially for space telescopes that operate in unserviceable orbits such as the James Webb Space Telescope (JWST), which is scheduled to be launched in 2018 and will operate at the Lagrangian point L2. JWST will be equipped with an active optics system to align each segment of its primary mirror and the secondary mirror, and to adjust the curvature of the primary mirror segments [7]. A prominent example of the necessity for active optics is the Hubble Space Telescope. Beside the well-known polishing error of its primary mirror, it was discovered that the alignment of Hubble's Wide-Field/Planetary Camera (WF/PC) was drifting over time. To tap Hubble's full potential, a subsequent service mission was scheduled to install a spare camera (WF/PC-2) which included optics to compensate for the polishing error of the primary mirror, and an actively controlled tip/tilt mirror to enable on-orbit alignment [8].

### *1.1. Active optics for space applications*

The active optics used in the Hubble Space Telescope and the JWST only allow for few degrees of freedom, which may not be sufficient to correct for the aberrations of even larger primary mirrors. Until now, active optics for space applications face an ongoing development. Beside new concepts which aim for active primaries [9, 10], the approach presented here uses deformable mirrors with many degrees of freedom for dedicated wavefront control at a plane conjugate to the primary mirror.

The first study conducted by the European Space Agency (ESA) on the topic of deformable mirrors for space applications was performed at the end of the 1990s in the course of the "Adaptive Optics Technology" research program. In the scope of this activity, a membrane micromachined deformable mirror (MMDM) with a clear aperture of 50 mm and a dedicated working aperture of 35 mm was developed for the correction of low-order Zernike modes with a stroke of several  $\mu\text{m}$  [11]. The mirror is well suited for the correction of low-order aberrations, it is lightweight, inexpensive, and exhibits only negligible hysteresis. However, it is difficult to scale the membrane mirror technology to much larger apertures, limiting its use for the correction of large primary mirrors. In [12], three MMDMs have been tested in thermal vacuum at cryogenic temperatures. The authors reported an increase of the non-spherical initial surface deviation from flat at 78 K, which was strong for two, and moderate but correctable for one of the tested mirrors. The mirrors were not specifically designed for cryogenic applications.

Another important technology is based on micro electrical mechanical system (MEMS) techniques [13, 14]. MEMS mirrors are lightweight, have low power consumption, and can be manufactured with a high actuator count. Their stroke is limited to a few micrometers. They enable high spatial frequency wavefront correction with negligible hysteresis, which renders these mirrors suitable for high precision wavefront correction in their regime. A MEMS deformable mirror has been tested in thermal vacuum at cryogenic temperatures [15]. Only small changes of the surface figure at 95 K were reported. MEMS deformable mirrors successfully underwent vibration tests, and a 32x32 element mirror was launched on board a sounding rocket in 2011 as part of an imaging instrument [16], showing that the technology is space compliant.

In 2003, a deformable mirror for space applications based on electrostrictive actuation was presented [17]. This stacked-array deformable mirror with an aperture of approximately 160 mm should operate at cryogenic temperatures between 35 K and 65 K. The specifically developed actuators delivered a stroke of approximately 3  $\mu\text{m}$  over the full designated temperature range. The drawbacks of this technology were the limited stroke of the mirror and the high mass of approximately 5.9 kg. Due to the strong temperature dependence of the used electrostrictive material, the actuation technology is limited to a rather small temperature range.

A more recent example is the MADRAS (Mirror Actively Deformed and Regulated for Applications in Space) deformable mirror [18]. Implementing a different design compared to previous deformable mirrors, MADRAS was specifically designed to correct for aberrations of a 3 m-class lightweight primary mirror in space environment. The mirror has an aperture of 90 mm and is able to create specific Zernike modes with a stroke up to 1  $\mu\text{m}$  with a high accuracy of better than 10 nm RMS deviation from the target surface. The actuator geometry mitigates actuator print-through, still provides sufficient correction capability in case of actuator failure, and includes means to clamp the mirror during launch. Influence of the space environment and the vibrations during launch have been assessed numerically, but no results from conducted tests have been published so far.

In the course of a project funded by ESA, we have developed and manufactured a deformable mirror based on piezoelectric actuation that is space compliant. This was a generic technology development for a deformable mirror which can be used in an active optics system for a future large space telescope. The mirror should deliver low order Zernike modes with surface peak-to-valley strokes of 30  $\mu\text{m}$  (60  $\mu\text{m}$  wavefront) in defocus mode, 5  $\mu\text{m}$  in trefoil mode, and diffraction limited surface quality over an aperture of 50 mm. It should operate in thermal vacuum at temperatures between 100 K and 300 K. Furthermore, the mirror should be able to withstand laser energy fluences up to 5 J/cm<sup>2</sup> at a wavelength of 1064 nm. To the best of our knowledge, at present there is no mirror with similar specifications that is space qualified.

### 1.2. Design considerations

For the required specifications, the unimorph design was identified as a suitable candidate. Unimorph deformable mirrors are compatible with apertures of 50 mm, which are difficult to achieve with membrane-based mirrors. They can be built from a small number of CTE-matched components, rendering them insensitive to temperature fluctuations. The mirror's stroke is determined by its aperture and thickness. Thin mirrors allow for large strokes, but are prone to stress-induced surface deformations, which have to be accounted for during the manufacturing process.

Unimorph and bimorph mirrors are actuated by forces which lie in a plane parallel to the mirror surface. Another actuation scheme is based on stiff actuators which facilitate actuation by generating forces perpendicular to the mirror surface. This scheme uses, for example, arrays of stacked actuators based on piezoelectric or electrostrictive materials. The achievable stroke of these stacked-array mirrors is roughly proportional to the actuator spacing. For example, a maximum surface peak-to-valley stroke of 7  $\mu\text{m}$  was achieved over an aperture of 49 mm with an actuator spacing of approximately 3.2 mm [19]. A surface peak-to-valley stroke of 30  $\mu\text{m}$  would require much larger apertures than 50 mm.

The unimorph design is compact and lightweight, since it does not rely on rigid support structures. Without such a structure on the other hand, the design is more prone to vibrations than stacked-array mirrors [20]. The use of superpolished prefabricated glass substrates furnished with a high-reflective dielectric coating also ensures high laser power handling capability.

A unimorph deformable mirror with specifications similar to the mirror we present here is currently being developed by CILAS [19]. It features 63 actuators and shall deliver a surface

peak-to-valley defocus stroke of  $25\ \mu\text{m}$  ( $50\ \mu\text{m}$  wavefront) over an aperture of approximately 85 mm while providing diffraction-limited surface quality. The mirror's front side is equipped with a space qualified silver protected coating developed by CILAS. It already underwent operational lifetime tests, results from environmental tests are expected at the end of 2016.

### 1.3. Unimorph deformable mirror

Design and manufacturing of our mirror were published in [21]. The main component is the unimorph mirror structure shown in Fig. 1. We refer to this as the "main mirror structure". It consists of a reflectively coated glass substrate which is bonded to a piezoelectric disc. The overall diameter of the glass substrate is 64 mm. Due to the simple unimorph design, the main mirror structures weighs only about 100 g. The area of the mirror that can be controlled with high precision has a diameter of 50 mm and is equal to the clear aperture of the assembled mirror.

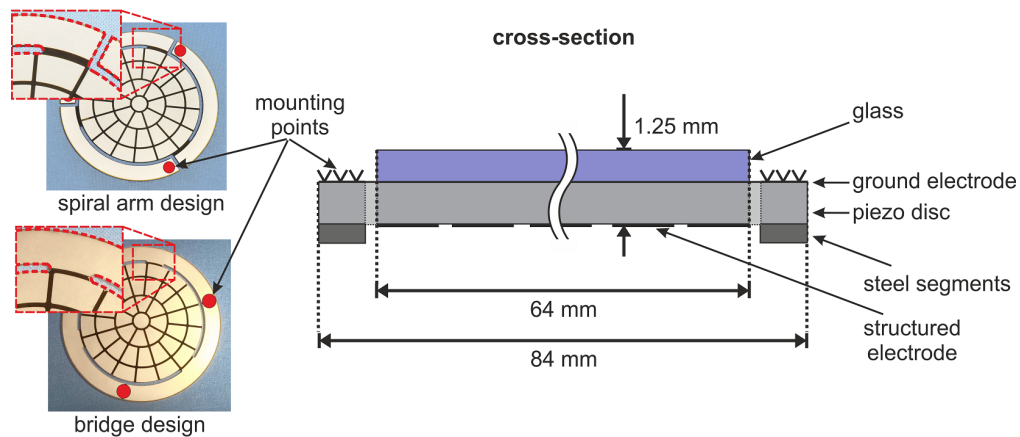


Fig. 1. Main mirror structure. Left: back side of the piezoelectric disc in the spiral arm design (top) and the bridge design (bottom). The difference between the two designs is highlighted by the dashed red lines in the insets that trace the contour of the piezoelectric disc. Mounting points are marked by the red dots. Right: schematic cross-section of the main mirror structure.

We studied two different designs of the piezoelectric disc, shown on the left side of Fig. 1: the "spiral arm" design, featuring large tip/tilt amplitudes, and the "bridge" design, which is mechanically stiffer at the cost of reduced tip and tilt. In the bridge design, the ends of the three spiral arms are connected to the junction of the next arm. This increases the stiffness of the arms, but restricts their bending capability. Since tip and tilt of the central disc is facilitated via unimorph actuation of the arms, this modification leads to the reduced tip/tilt amplitudes. The main mirror structure is glued to a mounting ring, which is fitted inside the mirror housing. All mechanical parts are made of the Fe-Ni alloy Kovar, which has a coefficient of thermal expansion similar to the piezoelectric material we use (PIC 151 from PI Ceramic) [22]. The mounted main mirror structure and the assembled mirror are shown in Fig. 2.

This generic mirror had to be compliant with vacuum, large temperature variations, cosmic radiation, high power laser irradiation, and vibrations imposed by the launch vehicle. ESA further demanded an operational temperature range from 100 K to 300 K. This paper reports on the tests conducted to assess the mirror's compliance with space environment and ESA's requirements.

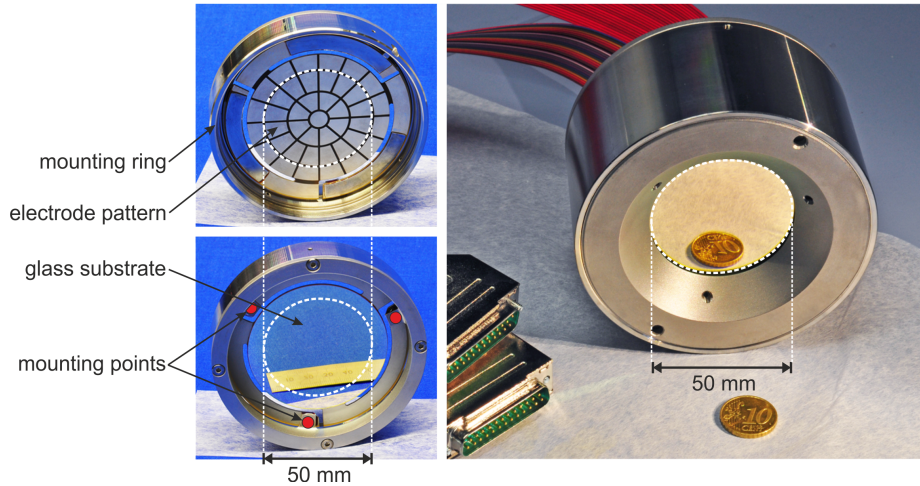


Fig. 2. Left: back side (top) and front side (bottom) of the main mirror structure in its mounting ring. The area of the mirror that can be controlled with high precision has a diameter of 50 mm and is marked by the dashed white circle. Right: fully assembled deformable mirror.

## 2. Environmental and performance tests

Three deformable mirrors, DM-1, -2, and -3 have been manufactured [21] and underwent different environmental and performance tests. Environmental tests were conducted according to the standards defined by the European Cooperation for Space Standardization (ECSS) [23].

### 2.1. Thermal vacuum

To determine the mirror's performance in vacuum at cryogenic temperatures, the first deformable mirror prototype (DM-1) was placed inside a vacuum chamber at EADS Astrium. Temperatures down to 77 K can be created inside the chamber by using liquid ( $\text{LN}_2$ ) or gaseous Nitrogen ( $\text{GN}_2$ ). A photograph of the deformable mirror placed in the inner shroud of the vacuum chamber is shown in Fig. 3.

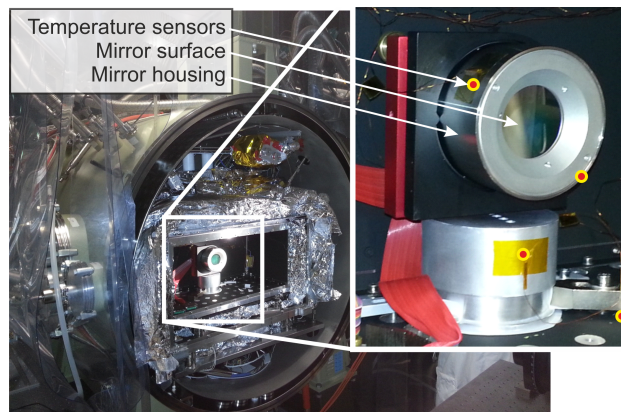


Fig. 3. Deformable mirror DM-1 mounted in the inner shroud of the thermal vacuum test chamber. Red dots indicate the positions of temperature sensors in proximity of the mirror.

A schematic view of the experimental setup, along with an image of the optical bench located in front of the vacuum chamber is shown in Fig. 4. The optical bench could be adjusted in 2 axes. All surface measurements were conducted at thermal equilibrium, using a high resolution Shack-Hartmann wavefront sensor (Optocraft WFS SHS Lab 130-GE-UHR) with 116 x 116 lenslets, and a clear aperture of 15.1 mm in diameter. The wavefront sensor uses an internal illumination module powered by a fibre-coupled diode laser with a wavelength of 635 nm. The sensor's absolute measurement accuracy is 22 nm RMS, the relative accuracy when calibrated against a reference flat is 3 nm RMS. A telescope consisting of two achromatic lenses with focal lengths of 310.64 mm and 80.4 mm is used to adapt the wavefront sensor's aperture to the 50 mm aperture of the deformable mirror. Image and object distances are chosen accordingly as to relay the deformable mirror surface onto the lenslet array of the Shack-Hartmann sensor. Astrium estimates the relative measurement accuracy of the whole setup with 8-10 nm RMS.

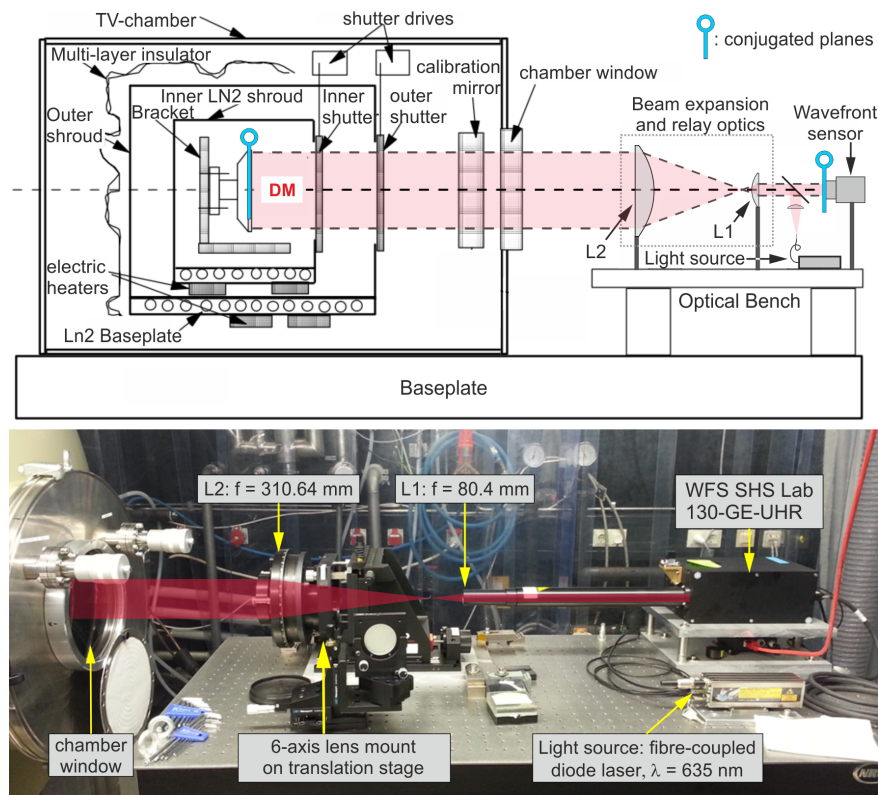


Fig. 4. Top: Schematic of the thermal vacuum performance verification test setup, not to scale. Bottom: Image of the optical bench located in front of the vacuum chamber. The optical setup on the bench consists of a Shack-Hartmann wavefront sensor with integrated illumination, and a beam expansion telescope consisting of lenses L1 and L2. The 6-axis mount of lens L2 is fixed onto a translation stage to adjust the telescope.

We assessed the mirror's performance at different temperatures by applying Zernike modes  $Z_3$  (defocus) to  $Z_{10}$  (trefoil  $30^\circ$ ) to the deformable mirror in closed-loop operation. Throughout this paper, we use the Zernike notation of Wyant and Creath [24]. For each temperature, the closed-loop operation of the mirror started at a surface peak-to-valley amplitude of  $0.5 \mu\text{m}$  for each Zernike mode. Ten loop iterations were permitted to achieve a residual RMS-deviation of the measured mirror surface from the target surface below  $\lambda/14$  ( $\lambda = 1064 \text{ nm}$ , Maréchal-

criterion). Upon successful measurement, the Zernike amplitude was raised by 10 % of the maximum Zernike amplitude of the respective mode (which was estimated prior to the tests) and the next measurement was made. This procedure was repeated until one of the following criteria arose: The residual RMS deviation from the targeted Zernike mode exceeded the Maréchal-criterion, or the required voltage exceeded the maximum allowed voltage of  $\pm 400$  V. In that way, the maximum Zernike amplitudes that the mirror can produce within the Maréchal limit, and the residual RMS-deviation from the targeted Zernike mode were determined.

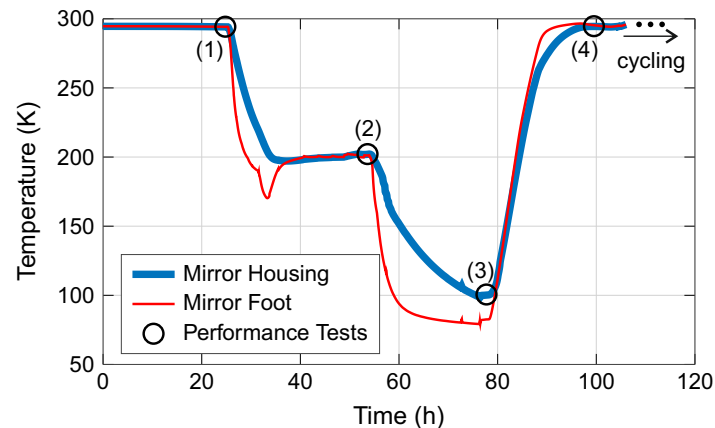


Fig. 5. Temperature profiles recorded by the temperature sensors indicated in Fig. 3 during one cycle. The positions of the surface measurements are indicated by black circles.

The first measurement was conducted in the evacuated test chamber at ambient temperature (approx. 294 K). Further measurements were conducted at 200 K, 100 K, and again at ambient temperature, after finishing one full thermal cycle. Figure 5 shows the temperature profile recorded by sensors attached to the mirror housing and its mounting foot. Black circles indicate that a measurement of maximum Zernike amplitudes as described above was performed. After this first cycle, 8 cycles between 100 K and 300 K without intermediate surface measurements were conducted. One final measurement was conducted after finishing the 8 cycles.

Figure 6 depicts the maximum Zernike amplitudes obtained during the first thermal cycle and those after 8 thermal cycles. As can be seen, the mirror was operating successfully at all temperatures. The maximum Zernike amplitudes decrease with decreasing temperature. Compared to the amplitudes achieved at room temperature, the amplitudes decrease to  $64 \pm 10$  % at 200 K and  $39 \pm 8$  % at 100 K. This is expected, since the piezoelectric coefficients decrease with decreasing temperature [25]. The decrease of the piezoelectric coefficient could potentially be compensated by using higher voltages, since the dielectric breakdown threshold of the piezoelectric ceramic increases with decreasing temperature [26]. For several Zernike modes, the maximum obtained Zernike amplitudes after the cycling are larger than the ones obtained before cycling. This is probably due to the fact that Zernike amplitudes were raised in steps of 10 % of the maximum amplitude. Finer steps may have resulted in smaller differences between the amplitudes before and after thermal cycling.

In [27], the temperature dependent defocus stroke of a unimorph structure using the same piezoelectric material that was used for our deformable mirror (PIC 151) is investigated. The authors report a decrease in stroke with decreasing temperature to approximately 68 % at 200 K, and 47.5 % at 86 K. The value at 200 K is in good agreement with our observations, the stroke at 86 K is slightly higher than what we observed. This can be explained by the different experimental procedures. In [27], a voltage of  $0.4 \text{ kV mm}^{-1}$  was applied to the unsegmented back

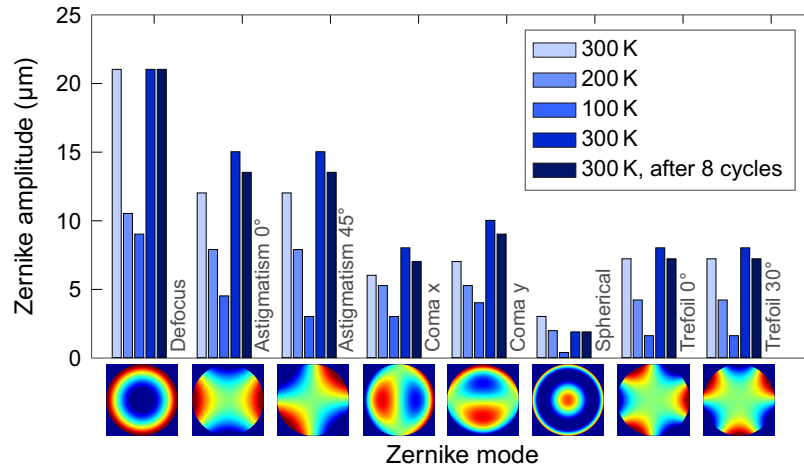


Fig. 6. Maximum Zernike amplitudes of DM-1 in thermal vacuum achieved at the performance tests indicated in Fig. 5 (300 K, 200 K, and 300 K). The last performance test at 300 K was conducted after eight thermal cycles between 300 K and 100 K.

side electrode of the unimorph structure at different temperatures. The surface figure of the generated shape was evaluated for peak-to-valley deformation, and for the generated amount of defocus. The contributions of additional Zernike modes to the total deformation was quantified in [28], but these contributions were not corrected for since the unimorph structure is not furnished with a segmented electrode. In our experiment, pure Zernike modes should be generated by the deformable mirror. The quality of the modes was determined by the Maréchal-criterion (RMS-deviation of the measured surface from the target surface has to be below  $\lambda/14$ ). If, to achieve the demanded surface figure, a larger amount of the available voltage range must be spent on the correction of thermally induced deformations at cryogenic temperatures, less voltage is available for the generation of the Zernike mode. In the following paragraphs, the amount of the thermally induced deformations is quantified.

At low temperatures, the unpowered residual surface deviation from best sphere increased by approximately  $1\ \mu\text{m}$  (peak-to-valley) at 200 K and  $5\ \mu\text{m}$  (peak-to-valley) at 100 K. The main contribution is of similar appearance as electrode print-through, and thus on spatial frequencies which cannot be corrected by actuation. This additional surface deviation originates from the same root as the electrode print-through. It can be explained by the anisotropic thermal expansion of the piezoelectric material PIC 151. The coefficient of thermal expansion (CTE) in the direction of the piezoelectric polarization is positive, whereas the CTE in directions perpendicular to the poling direction is negative. As was pointed out in [21], the first mirror prototypes exhibited a different piezoelectric polarization in the gaps between the mirror's electrodes compared to the area underneath an electrode. This polarization inhomogeneity resulted in print-through, and leads furthermore to an inhomogeneous CTE. Hence, a temperature change yields different thermal expansion between these regions, thereby magnifying the already visible electrode print-through. The newest manufactured mirror prototypes presented in [21] exhibit significantly less print-through than the mirror tested here. We expect the temperature dependent increase of the residual surface deviation from best sphere to be significantly reduced in the newer mirrors, but these have not been tested at cryogenic temperatures yet.

The curvature of the mirror changed with temperature due to the small CTE mismatch between the piezoelectric disc and the glass substrate. The initial (concave) radius of curvature  $R$  of approximately 9.1 m at 294 K changed to 6.7 m at 200 K and 4.5 m at 100 K. After cycling,

the mirror returned to its initial curvature. The corresponding defocus coefficients ( $Z_3$ ) can be calculated from the radii of curvature  $R$  and the mirror aperture radius  $r$  via  $Z_3 = r^2/4R$ . The CTE difference  $\Delta\alpha$  between the piezoelectric disc and the glass substrate can then be derived from the defocus coefficient  $Z_3$  via

$$\Delta\alpha = 2Z_3 \cdot \frac{t_p^4 E_p^2 + 4t_p^3 E_p t_g E_g + 6t_p^2 E_p t_g^2 E_g + 4t_g^3 E_g t_p E_p + t_g^4 E_g^2}{3t_p E_p t_g E_g (t_p + t_g) r^2 \Delta T} \quad (1)$$

[29], where  $E_p = 67$  GPa and  $E_g = 71$  GPa are the Young's moduli of the piezoelectric material PIC 151 and the glass material (N-BK10 from Schott),  $t_p = 700\mu\text{m}$  and  $t_g = 550\mu\text{m}$  are the thicknesses of the piezoelectric disc and the glass substrate, and  $\Delta T$  is the temperature difference between the measurements. Equation (1) yields a CTE mismatch of  $\Delta\alpha_{294\text{K}-200\text{K}} = 0.35 \times 10^{-6} \text{K}^{-1}$  between 294 K and 200 K, and a CTE mismatch of  $\Delta\alpha_{200\text{K}-100\text{K}} = 0.61 \times 10^{-6} \text{K}^{-1}$  between 200 K and 100 K. In [22], the CTE mismatch at room temperature (294 K) was measured to  $\Delta\alpha_{294\text{K}} = -0.08 \times 10^{-6} \text{K}^{-1}$ . Results from extensive measurements of the CTE of the material PIC 151 between 293 K and 86 K are presented in [27]. Care has to be taken when comparing CTE measurements of the used soft PZT material. According to the vendor (PI Ceramic), the CTE may differ between different batches.

Deformation due to the remaining CTE mismatch between the piezoelectric disc and the Kovar mounting ring onto which the disc is glued was not observed. This can be attributed to our special three-arm design which averts mounting stress, see [21].

In summary, we have shown that our unimorph deformable mirror withstands thermal cycling between 294 K and 100 K, and successfully operates at all temperatures in that range. When working with such large operation temperature ranges, careful design as well as CTE matching both by material selection and material preparation is vital to mitigate unwanted surface deformations.

## 2.2. Vibration

Deformable mirrors with two different main mirror structures as described in [21] were tested to assess the mirror's behavior under vibration load: The spiral arm design with a  $700\mu\text{m}$  thick piezoelectric disc, as well as the bridge design with two piezoelectric disc thicknesses ( $700\mu\text{m}$  and  $1000\mu\text{m}$ ).

Acoustic tests have been conducted to verify the frequency of the numerically obtained eigenmodes of the two different main mirror structures. For this purpose, the mirror was subjected to sinusoidal sound waves generated by a speaker. The frequency was increased from 50 Hz to 2000 Hz. The frequency response was measured by recording the voltage which was generated by the vibrating mirror structure due to the piezoelectric effect. Figure 7 shows the response of both mirror structures (spiral arm and bridge design,  $700\mu\text{m}$  thick) to the sinusoidal acoustic excitation. The experimental results are in good agreement with the numerical simulations. The first eigenmode of both mirror designs is a piston-like movement perpendicular to the mirror surface, with a frequency of 82 Hz and 226 Hz for the spiral arm design and the bridge design, respectively. Thus, stiffening the mirror structure by using the bridge design was successful, leading to an almost three times higher frequency of the first eigenmode.

Vibration tests have been carried out at the European Space Research and Technology Centre (ESTEC). Each mirror was subjected to sinusoidal and random vibrations with increasing vibration levels. The final vibration test levels for each axis are listed in Table 1. Sinusoidal vibration test levels were increased from 33 % to 100 % of the final vibration test levels in steps of 33 %, random vibration test levels were increased from 25 % to 100 % in steps of 25 %. After each step, the mirror was inspected for damage visually and by measuring the electrical capacitance of its actuators. A fracture in the mirror structure or a damage to the electric connections

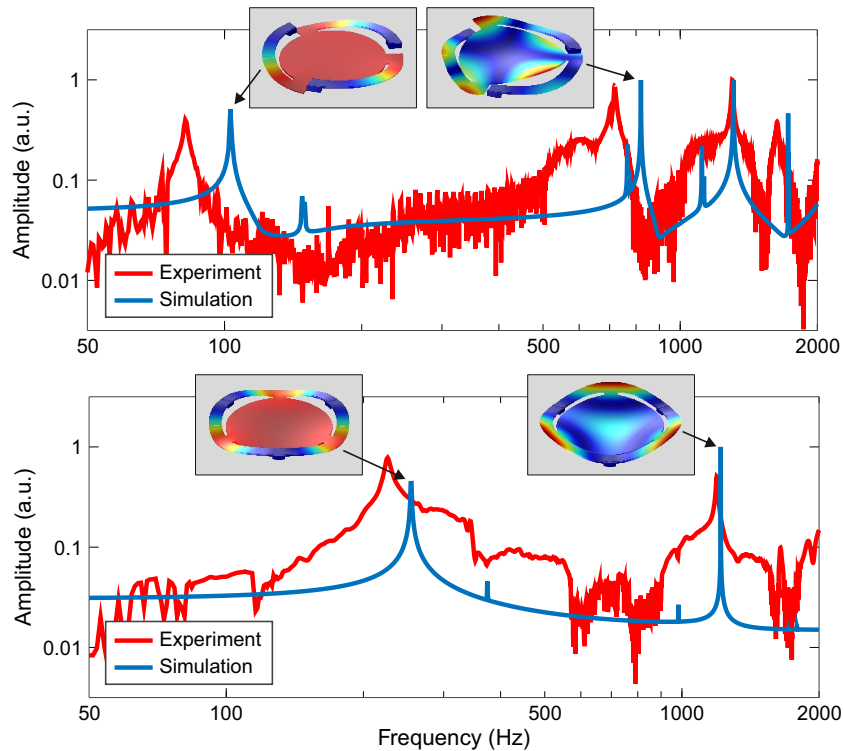


Fig. 7. Measured (red) and calculated (blue) response of the main mirror structure in the spiral arm design (top) and in the bridge design (bottom) to acoustic sinusoidal excitation normal to the mirror surface. The insets show the (calculated) shape of the first two dominant eigenmodes of each design. For both designs, the first eigenmode corresponds to a piston-like movement of the central disc.

is accompanied by a decrease of the actuator capacitance.

For each type of vibration, two vibration directions were tested. The  $z$ -direction corresponds to the direction normal to the mirror surface. Due to the cylindrical symmetry of the mirror assembly, the  $x,y$ -directions had an arbitrary orientation in the plane perpendicular to the  $z$ -direction. The first mirror design (spiral arm design) failed at 100 % of the random vibration in the  $x,y$ -direction after 110 s. It was not tested in the  $z$ -direction. The fracture occurred at the junction between the arms and the central disc, probably due to high stress caused by resonant excitation of a low order eigenmode of the main mirror structure during the test. An image of the fracture site, along with results from a numerical stress analysis is shown in Fig. 8.

Both mirrors which were manufactured in the bridge design passed the sinusoidal vibration tests in both axes, as well as the random vibration test in the  $(x,y)$ -direction at full levels (14.1 g RMS). Full random vibration levels in the  $z$ -direction were not reached, the mirror structure withstood only up to 50 % (9.3 g RMS) of the final level. Random vibration levels of common launcher vehicles are, for example, 4.94 g RMS for the Soyuz launcher [30], and 7.3 g RMS for the Ariane 4 [31]. Qualification and acceptance levels are higher, e.g. 11 g RMS for an Ariane 5 auxiliary payload. Depending on the used launcher vehicle, the deformable mirrors manufactured in the bridge design should be compliant with the required vibration loads.

The fact that the bridge design withstood much higher loads than the spiral arm design shows that the mirror's resistance towards vibration can be increased by simple structural modifica-

Table 1. Vibration test levels

Type	Frequency (Hz)	Sweep rate	Vibration spectrum	Final Level/Duration
<b>Sinusoidal vibration (all directions)</b>	5-21	2 Oct/min	-	11 mm amplitude 20 g 6 g
	21-60			
	60-100			
<b>Random vibration (x, y)</b>	20 - 100	3.0 dB/Oct	0.06 - 0.2 g <sup>2</sup> /Hz	14.1 g RMS, 120 s
	100 - 400	0.0 dB/Oct	0.2 g <sup>2</sup> /Hz	
	400 - 2000	-3.0 dB/Oct	0.2 - 0.01 g <sup>2</sup> /Hz	
<b>Random vibration (z)</b>	20 - 100	3.0 dB/Oct	0.06 - 0.35 g <sup>2</sup> /Hz	18.6 g RMS, 120 s
	100 - 400	0.0 dB/Oct	0.35 g <sup>2</sup> /Hz	
	400 - 2000	3.0 dB/Oct	0.35 - 0.01 g <sup>2</sup> /Hz	

Direction 'z' corresponds to the direction perpendicular to the mirror surface. Note that for random vibrations, final levels are the integrated acceleration spectral densities.

tions. Thus, the prospects are good to make the bridge design resistant to the full 18.6 g RMS random vibration in z-direction by further modifications. One such modification could be increasing the thickness of the three arms. This would increase the eigenfrequencies of the whole structure at the cost of tip/tilt amplitude. We have conducted finite element analysis to assess the impact of increasing the arm thickness by 1 mm. The maximum amplitude for low order Zernike modes would decrease by approximately 10%. At the same time, the first eigenfrequency is shifted from 250 Hz to 600 Hz, which renders the main mirror structure much more resistant towards vibration.

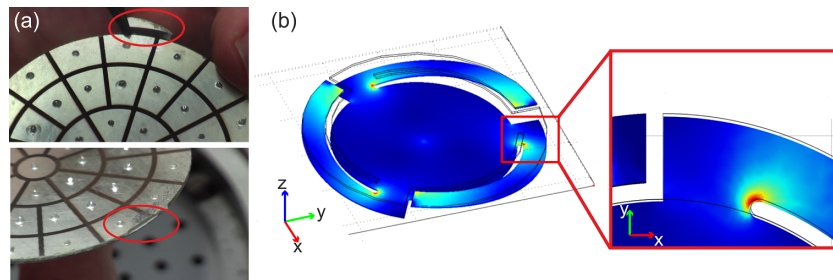


Fig. 8. (a) Fracture site of the spiral arm design after the random vibration test (DM-1). (b) Numerical calculation of the von-Mises stress inside the main mirror structure induced by the excitation of the first eigenmode.

The vibration tests during which the deformable mirror DM-1 was irreparably damaged were performed after the performance tests in thermal vacuum. Hence, a different mirror had to be used for the remaining tests. For most of the tests the deformable mirror DM-2 was used, except for the proton irradiation tests. These tests required the radioactivity of the mirror to decay to safe radiation levels afterwards, which took several weeks.

### 2.3. Ionizing irradiation

The mirror was submitted to ionizing irradiation to assess its impact on the electromechanical response of the PZT-ceramic. In [32], a high tolerance of PZT-ceramics towards  $\gamma$ -radiation and  $\beta$ -radiation is reported, only limited by excessive heating induced by high flux levels, which lead to depolarization and thus loss of actuator stroke. Radiation-induced brittleness of

the used adhesives may also lead to a loss of stroke, or entire failure of actuation. To assess the impact on the mirror performance, the stroke of each actuator before and after the irradiation is compared.

### *Gamma irradiation*

The deformable mirror DM-2 was subjected to gamma irradiation at ESTEC's Cobalt-60 facility. A total dose of 50 krad was applied to the mirror, the dose rate was  $1 \text{ krad h}^{-1}$ . No shielding was used, and the tests were conducted at atmospheric pressure and room temperature.

### *Proton irradiation*

The deformable mirror DM-3 was subjected to proton irradiation at the Proton Irradiation Facility (PIF) of the Paul-Scherrer Institute (PSI, Switzerland). The proton beam at the position of the deformable mirror was collimated and had a flat-top profile with a diameter of approximately 58 mm. The mirror was centered behind the collimator to irradiate the 50 mm optical aperture. A proton energy of approximately 30 MeV was incident on the mirror surface. The proton flux was kept constant around  $7 \times 10^6 \text{ s}^{-1} \text{ cm}^{-2}$ . The total integrated fluence was  $1 \times 10^{11} \text{ cm}^{-2}$ . To assess the influence of different fluences, half of the mirror aperture was covered by a 10 mm thick aluminum plate to reduce the fluence to approximately 50 %.

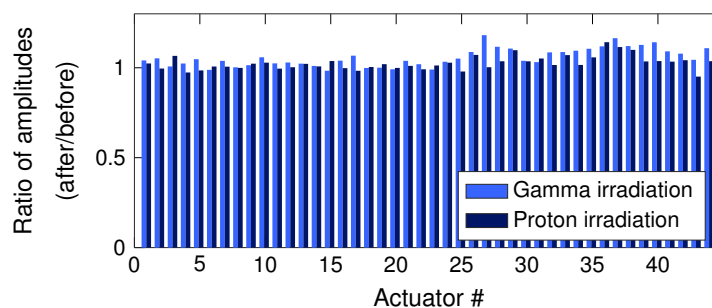


Fig. 9. Ratio of the peak-to-valley amplitudes of each actuator for a voltage of 100 V prior and after the gamma- and proton-irradiation tests.

### *Performance after irradiation*

Figure 9 shows the ratio of the peak-to-valley amplitudes of the individual actuators prior and after the irradiation. As can be seen, no actuator was damaged. The mean amplitude ratio is 106 % for the gamma irradiation test, with a standard deviation of 5.0 %, and 103 % for the proton irradiation test, with a standard deviation of 3.8 %. The used material PIC 151 exhibits a piezoelectric hysteresis of approximately 15 %, hence the scatter of the amplitude ratio is well within the limits given by hysteresis. The mirror is thereby compliant with the tested levels of ionizing irradiation.

## **3. Operational tests**

### *3.1. Laser irradiation*

ESA required testing the mirror's laser power handling capability to assess its suitability for high power applications, such as Light Detection and Ranging (LIDAR). The damage threshold had to be larger than  $5 \text{ J/cm}^2$ , and the mirror had to withstand an average intensity up to  $500 \text{ W/cm}^2$ . Two damage mechanisms are of interest: Laser-induced damage of the coating,

and heating of the mirror. Excessive heat might degrade the adhesive layer between glass substrate and piezoelectric disc. Additionally, as the temperature of the piezoelectric disc increases towards the Curie temperature of the PZT ceramic (250 °C [33]), depolarization will occur.

To test for high energy fluence, we focused laser light from a Thales SAGA 220/10 laser system on the surface of the deformable mirror DM-2. The system delivers pulse energies up to 1 J at a pulse duration of 6 ns and a repetition rate of 10 Hz. The spot diameter on the mirror surface was changed to vary the energy fluence. The deformable mirror DM-2 was subjected to pulses with an energy of 770 mJ, focused to a spot of approximately 4.1 mm in diameter, which results in a fluence of 5.8 J/cm<sup>2</sup>. The beam profile exhibited hot spots, therefore local energy fluences within the laser spot might have been much higher. To assess the damage threshold, the test was repeated with one of the structural models which were previously manufactured and are furnished with identical dielectric coatings. The spot size was reduced from 4.1 mm to 2.8 mm in diameter, where the coating was damaged. The calculated fluence at that spot size was approximately 12.5 J/cm<sup>2</sup>.

To assess the high average power handling capability, we focused laser light from a TRUMPF thin-disk laser upon the surface of the deformable mirror DM-2. The system delivered an average power of 100 W in continuous-wave operation, the mirror was exposed for 30 s. We increased the laser beam intensity by decreasing the spot size on the mirror from 6 mm down to 3 mm, which corresponds to an intensity of 1415 W/cm<sup>2</sup>. Three different positions on the mirror surface were irradiated.

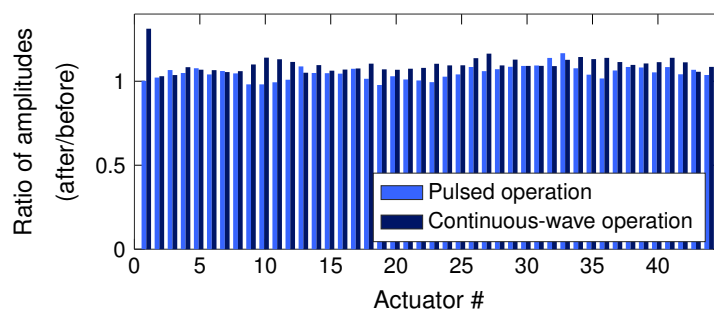


Fig. 10. Ratio of the peak-to-valley amplitudes of each actuator for a voltage of 100 V prior and after the laser irradiation tests.

The peak-to-valley amplitudes of each actuator before and after the tests was compared in the same manner as for the ionizing irradiation test, the results are shown in Fig. 10. As can be seen, no significant change in actuator response was detected. The mean amplitude ratio is 105 % for the high energy fluence test, with a standard deviation of 4.0 %, and 110 % for the high average power test, with a standard deviation of 4.5 %. The scatter of the amplitude ratio is again well within the limits induced by piezoelectric hysteresis. The mirror surface was inspected for damage or local deformation after the test, but none could be detected.

### 3.2. Operational life time

We assessed the long-term functionality of the deformable mirror by applying a sinusoidal voltage with a frequency of 15 Hz and an amplitude of 350 V. The voltage was applied to all electrodes of DM-2 simultaneously. This voltage pattern represents the maximum electromechanical load that the mirror can be driven with, and roughly corresponds to the Zernike mode Z<sub>3</sub> (defocus).

The control signal was applied for 8 days, which corresponds to approximately 11 million full cycles. The peak-to-valley amplitudes of each actuator before and after the test was compared

in the same manner as for the ionizing irradiation and laser irradiation tests, the results are shown in Fig. 11. As can be seen, every electrode is still operating. The mean amplitude after

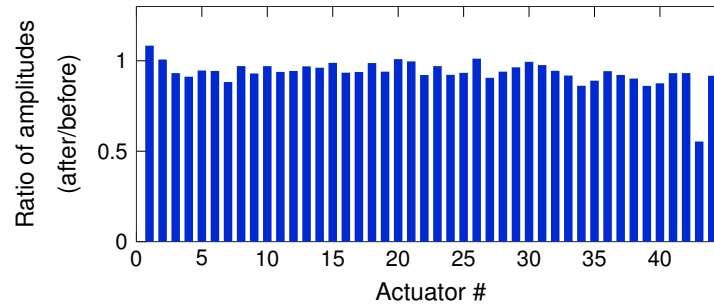


Fig. 11. Ratio of the peak-to-valley amplitudes of each actuator for a voltage of 100 V prior and after the continuous operation test.

the test decreased to 94 % of the value prior to testing, with a standard deviation of 7.3 %. Before the long-term functionality test, the standard deviation of the peak-to-valley amplitudes of each actuator was 2.9 %. The increase in the deviation is mainly attributed to the amplitude of actuator 43, which decreased to 55 % after the test, and remained at this level. The drop in amplitude was accompanied by an increased electrical resistance of the actuator connection. After reestablishing the connection, the amplitude increased to approximately 90 % of the initial amplitude, yielding a standard deviation of the amplitude ratios of 4.3 %. The difference of the deviations before and after the tests are again within the limits induced by piezoelectric hysteresis.

#### 4. Conclusion

We have presented environmental and performance tests of a unimorph deformable mirror. The mirror had to deliver low order Zernike modes with an amplitude of several tens of  $\mu\text{m}$  and high surface fidelity, and be compliant with a space environment. Submission to ionizing gamma and proton irradiation did not yield an observable degradation of the actuator stroke or the surface quality. It was shown that the mirror is vacuum compatible and able to operate between room temperature and 100 K. It successfully underwent 9 thermal cycles between 100 K and 294 K, during which performance tests regarding stroke and surface fidelity were conducted. Laser irradiation tests revealed that the mirror withstands intensities up to  $1415 \text{ W/cm}^2$  in continuous-wave operation and energy fluences larger than  $5.8 \text{ J/cm}^2$  in pulsed operation. In conclusion, the conducted tests have shown that the mirror is compliant with natural space environment. Having demonstrated its operability in a relevant environment, we consider the mirror technology matured to a technology readiness level (TRL) 5.

The mirror structure passed all but one vibration tests at qualification levels. The failure occurred for random vibration in z-direction, at which 50 % of the final levels were reached. The damage was caused by resonant excitation of the mirror's first eigenmode at low frequency. This could be overcome by a structural modification to shift the eigenfrequencies towards higher values, thus rendering the mirror less sensitive to vibrations and further increasing its space compliance.

#### Acknowledgments

The authors gratefully acknowledge support for the work presented by the European Space Agency under contract number 4000104030/10/NL/EM.